Mo-promoted Pd/NaY catalyst for indirect oxidative carbonylation of methanol to dimethyl carbonate

Ke Huang, Shicheng Yuan, Rongyan Mei, Ge Yang, Peng Bai, Hailing Guo, Chunzheng Wang, Svetlana Mintova

Mo-promoted Pd/NaY catalyst for indirect oxidative carbonylation of methanol to dimethyl carbonate

Ke Huang,[a] Shicheng Yuan,[a] Rongyan Mei,[a] Ge Yang,[b] Peng Bai,[a] Hailing Guo,[a] Chunzheng Wang,*,[a] and Svetlana Mintova*,[a],[c]

[a] *State Key Laboratory of Heavy Oil Processing, College of Chemistry and Chemical Engineering, China University of Petroleum (East China), Qingdao 266580, Shandong, China*

[b] *College of Chemical Engineering, Qingdao University of Science and Technology, Qingdao 266042, Shandong, China*

[c] *Laboratoire Catalyse et Spectrochimie (LCS), Normandie Université, ENSICAEN, UNICAEN, CNRS, 6 boulevard Maréchal Juin, Caen 14050, France*

* Corresponding authors. E-mail addresses: czwang@upc.edu.cn (C. Wang), svetlana.mintova@ensicaen.fr (S. Mintova)

Abstract

A chlorine-free catalyst consisting of zeolite Y modified with Pd (Pd/NaY catalyst) has been prepared and used in the indirect oxidative carbonylation of methanol to dimethyl carbonate (DMC). The activity and stability of the catalyst were further improved by introducing molybdenum into Pd/NaY using a top-down approach (Pd-Mo/NaY catalyst). The Pd-Mo/NaY catalyst exhibited higher stability compared to the Pd/NaY. A high CO conversion of 97% and DMC selectivity of 80%

during a 30-hour catalytic test for the Pd-Mo/NaY were obtained. Furthermore, the incorporation of Mo was found to partially heal the silanols and hinder the aggregation of Pd in the Pd-Mo/NaY catalyst. The interactions between Mo and Pd increased the amount of active Pd^{2+} species and enhanced the adsorption of CO reactant on the Pd-Mo/NaY catalyst. The key reaction intermediate of $COOCH_3$* was captured by *in situ* DRIFTS spectra. The stabilization of active Pd^{2+} species contributed to the enhanced catalytic activity of the Pd-Mo/NaY catalyst in the indirect oxidative carbonylation of methanol to DMC reaction.

Keywords: Zeolite; NaY; Palladium; Carbonylation; Dimethyl carbonate

1. Introduction

Dimethyl carbonate (DMC) is an important raw chemical and intermediate due to its superior solubility, biodegradability and low toxicity.[1-3] Besides the main application for polycarbonate synthesis, DMC can be used as an electrolyte in lithium-ion batteries, fuel additives, and carbonylation and methylation reagents.[4-7] The main routes of DMC synthesis include: (i) phosgenation, (ii) direct or indirect oxidative carbonylation of carbon monoxide, oxygen, and methanol, (iii) direct synthesis from carbon dioxide and methanol, and (iv) transesterification of ethylene oxide, and (v) urea methanolysis.[8-10] Among these methods, the indirect oxidative carbonylation of methanol to DMC has attracted ever-growing attention due to the

safety issue (no risk of explosion), mild reaction conditions and high atom efficiency.[2]

In the indirect oxidative carbonylation of methanol to DMC, the common Pd-based catalysts as chlorine-containing and chlorine-free are used. In the case of chlorine-containing catalysts, the $PdCl_2$-$CuCl_2$/γ-Al_2O_3 showed an excellent initial DMC selectivity.[11,12] However, the loss of chlorine element due to the formation of CH_3OCOCl byproduct resulted in a rapid deactivation of the catalyst.[13] Therefore, considerable efforts have been devoted to the development of the chlorine-free Pd-based catalysts for DMC synthesis.[8,9,11,12,14-17] Tan et al. fabricated a high-performance Pd/NaY catalyst by using palladium acetylacetonate [$Pd(acac)_2$] complex as a precursor. The $acac^-$ ligand possibly promoted the re-oxidation of intermediate Pd species, and the catalytic activity of the Pd/NaY was related to the high oxidation state of Pd species.[14] Ji et al. reported that a single-atom Pd_1/TiO_2 catalyst contributed to significant improvement of catalytic performance. The steric hindrance effect of single-atom sites enhanced the DMC selectivity, as there was no extra Pd species resulting in the formation of byproduct.[15] Furthermore, Tan et al. revealed that mononuclear-isolated Pd^{2+} sites rather than aggregated Pd^0 centers led to the formation of DMC. The six-membered rings of zeolite NaY were responsible for isolating and stabilizing the Pd^{2+} sites.[16] These results suggest that the catalytic performance is associated with the oxidation state of Pd species.

It was demonstrated that the Pd^{2+} species were easily reduced to Pd^0 by the CO reactant, and thus the Pd sintering occurred during the catalytic reaction, which led to the catalyst inactivation.[4,5] To maintain the oxidation state of Pd species in the

chlorine-free catalysts, the effects of catalyst promoters such as K, Cu and Ga have been investigated.[17-19] Dong et al. found that the electron density of Pd species was enhanced in the presence of K promoter, and thus CO reactant was effectively activated due to the formation of a Pd–CO···K^+ structure.[17] Guo et al. developed a Cu-doped Pd/NaY catalyst with high catalytic performance. The Cu promoter improved the dispersion of Pd with abundant Pd^{2+} species.[18] A series of Ga-substituted NaY zeolites with controllable acidity and electron density of Pd^{2+} was reported by Wu et al.[19] With the Ga incorporation, the optimal electron density of Pd^{2+} enhanced the adsorption and activation of CO reactant and thus improved the formation of $COOCH_3$* intermediate.

Although considerable attention was paid to the optimization of the active Pd^{2+} species, the effect of silanol defects in the zeolite support have not been systematically discussed.[9,17-19] A single-site Mo-containing zeolites with controlled silanol defects was reported recently.[20-23] The insertion of Mo in the MFI structure contributed to low silanol content thus improving the hydrophobicity of the catalyst.

In this work, a Mo-modified Pd/NaY catalyst (Pd-Mo/NaY) was synthesized and applied in the indirect oxidative carbonylation of methanol to DMC. The Pd-Mo/NaY catalyst was prepared by a top-down method. The interactions between Mo and Pd in the Pd-Mo/NaY catalyst were studied by kinetic experiments, a series of *in situ* IR spectroscopy, H_2-TPR and XPS. The Pd-Mo/NaY catalyst exhibited excellent catalytic activity with CO conversion of 97% and DMC selectivity over 80% through 30 hours' catalytic test.

2. Experimental

2.1 Materials

Sodium hydroxide (NaOH, 96.0 wt%) and sodium molybdate dihydrate ($Na_2MoO_4 \cdot 2H_2O$, 99.0 wt%) were purchased from Sinopharm Chemical Reagent Co., Ltd. Sodium aluminum oxide ($NaAlO_2$, 98.0 wt%) was bought from Shanghai Aladdin Bio-Chem Technology Co., Ltd. Colloidal silica ($mSiO_2 \cdot nH_2O$, 30.0 wt%) was obtained from Qingdao Haiwan Specialty Chemicals Co., Ltd. Tetraamine dichloropalladium (II) monohydrate ($Pd(NH_3)_4Cl_2 \cdot H_2O$, 40.0 wt% Pd) was purchased from Macklin Biochemical Co., Ltd. All reagents were used directly without further purification.

2.2 Catalysts preparation

NaY zeolite: The NaY zeolite was synthesized according to the procedure previously reported.[24] 3.340 g NaOH was dissolved in 22.000 g deionized water and then 2.000 g $NaAlO_2$ was added into the solution. After stirring for 4 h, 24.310 g colloidal silica was added dropwise into the clear solution. The mixture was aged for 2 h at 25 °C, and then transferred into a 50 mL Teflon-lined autoclave and subjected to heating at 100 °C for 48 h under static condition. The solid product was collected by centrifugation at 5000 rpm for 10 min, purified with deionized water and dried at 80 °C for 12 h.

Mo/NaY zeolite: 3.000 g NaY zeolite was mixed with a solution containing 0.500 g $Na_2MoO_4 \cdot 2H_2O$ and 50 mL deionized water in a polypropylene bottle. The mixture was heated to 90 °C and stirred for 24 h. Then the suspension was centrifuged, purified and dried at 80 °C for 12 h. After that, the solid product was calcined at 550 °C for 5 h in air.

Pd/NaY and Pd-Mo/NaY catalysts: the introduction of palladium was performed as follow: 0.025 g $Pd(NH_3)_4Cl_2 \cdot H_2O$ was dissolved in 4.000 g deionized water. The Mo/NaY zeolite suspension was prepared by mixing 1.000 g of Mo/NaY zeolite and 96 mL deionized water in a three-necked flask and stirred for 2 h at 25 °C. After that, the $Pd(NH_3)_4Cl_2$ solution was added dropwise into the Mo/NaY zeolite suspension. Subsequently, the mixture was heated to 80 °C and stirred for 6 h. The solid product was separated by centrifuging, washed and dried for 12 h at 80 °C, followed by calcination in air at 200 °C for 2 h with a heating rate of 0.5 °C min^{-1}. Thus, the Pd-Mo/NaY catalyst was obtained.

A reference Pd/NaY catalyst was prepared following the same procedure using NaY zeolite as a support.

2.2 Characterization

Powder X-ray diffraction (XRD) patterns were recorded on a Bruker D8 Advance diffractometer equipped with a monochromated Cu Kα radiation (40 kV, 40 mA). The patterns were collected in a range of $2\theta = 5-60°$ with a scan rate of 1.2° min^{-1}.

N_2 adsorption isotherms of the samples were obtained at −196 °C with a

Quantachrome Autosorb-1 analyzer. The samples were degassed under vacuum at 300 °C for 2 h prior to the measurement. The specific surface area and microporous volume were calculated using the multi-point Brunauer-Emmett-Teller (BET) method and *t*-plot method.

Scanning electron microscopy (SEM) images were taken on a JEOL JSM-7900F instrument equipped with an energy dispersive X-ray spectrometer (EDS). Transmission electron microscopy (TEM) images were acquired using a Thermo Scientific Talos F200X TEM instrument. High-angle annular dark-field scanning transmission electron microscopy (HAADF-STEM) images and elemental mapping were performed using the same instrument equipped with an energy dispersive X-ray spectrometer (EDS). The chemical composition of the catalysts was determined by inductively coupled plasma optical emission spectroscopy (ICP-OES) on an Agilent 720 ICP-OES.

Thermogravimetric-mass spectrometry (TG-MS) was conducted on a NETZSCH STA 449 F5 instrument equipped with a QMS 403D mass spectrometer. The test was carried out under air atmosphere with a flow rate of 50 mL min^{-1} and a heating rate of 10 °C min^{-1}.

X-ray photoelectron spectroscopy (XPS) analysis of samples was performed on an Escalab 250xi spectrometer quipped with an Al Ka radiation (1486.7 eV).

The *in situ* transmission Fourier transform infrared (FT-IR) spectra of the catalysts were collected on a Bruker VERTEX 70V spectrometer with a resolution of 4 cm^{-1} over 64 scans. Wafers of compressed samples (15–20 mg) with a diameter of 13 mm

were placed in an infrared cell. Prior to the measurements, all samples were activated in vacuum at a heating rate of 10 °C min^{-1} up to 450 °C and evacuated for 1 h at 450 °C. After cooling to 25 °C, the samples were saturated with pyridine for 1 h at 25 °C. Subsequently, the samples were evacuated at 150 °C to remove the excess of pyridine molecules and the FT-IR spectra were recorded.[8,25] In addition, the CO adsorption spectra at −140 °C were recorded using the same spectrometer. The self-supporting pellets were inserted into the low-temperature infrared cell and activated at 450 °C for 1 h. After cooling to 25 °C, liquid nitrogen was added into the trap to cool down the connected cell. When the temperature of the cell reached −140 °C, pure CO gas was introduced gradually (CO partial pressure from 132−385 Pa) in vacuum and the spectra were recorded at different partial pressures.

Diffuse reflectance infrared Fourier transform spectroscopy (DRIFTS) experiments were performed using a Bruker Vertex 70V spectrometer equipped with a liquid N_2 cooling mercury-cadmium-telluride (MCT) detector and a home-made cell (ZnSe windows). For reactant CO adsorbed on the catalysts, the powder sample was pretreated in the cell under N_2 flow (50 mL min^{-1}) at 150 °C for 1 h and then cooled down to 35 °C to collect the background. Pure CO gas was introduced at 30 mL min^{-1} and maintained for 30 min. The sample was flushed by N_2 (50 mL min^{-1}) for 1 h and then the DRIFTS spectrum was collected at a resolution of 4 cm^{-1} over 32 scans. For *in situ* DMC synthesis, the powder sample was pretreated in the N_2 flow (50 mL min^{-1}) for 1 h at 200 °C and then cooled down to appointed temperature to record the background. Then a gas mixture of CO: CH_3ONO: N_2 (1: 6: 33; mole) was introduced

to the reaction cell at 30 mL min^{-1} for 15 min, and flushed with N_2 (30 mL min^{-1}) at appointed temperature for 15 min. The DRIFTS spectra before and after the N_2 purge were collected in the temperature range of 30–125 °C at a resolution of 4 cm^{-1} over 32 scans.

The H_2-temperature programmed reduction (H_2-TPR) was carried out in a Tianjin Xianquan TP-5080 apparatus equipped with a thermal conductivity detector. 0.100 g sample was pretreated in the flowing He at 200 °C for 1 h. Then the sample was cooled down to 30 °C and heated from 30 °C to 650 °C with a rate of 10 °C min^{-1} in a 10 vol% H_2/N_2 flow of 30 mL min^{-1}. The temperature programmed desorption of ammonia (NH_3-TPD) of the samples was performed on the same apparatus used for the H_2-TPR experiment. 0.100 g sample was loaded into a quartz tube and pretreated under He flow (50 mL min^{-1}) for 1 h at 500 °C. Subsequently, the sample was cooled down to 70 °C and saturated with 10 vol% NH_3/He under flow (30 mL min^{-1}), followed by purging with He (50 mL min^{-1}) for 0.5 h to remove physically adsorbed NH_3. Finally, the sample was heated to 650 °C under He flow (50 mL min^{-1}) with a heating rate of 10 °C min^{-1}.

2.3 Reactivity tests

The activity of the catalysts in the indirect oxidative carbonylation of methanol to DMC reaction was measured using a continuous-flow fixed-bed microreactor with a quartz tube (36 mm length by 8 mm inner diameter) under 0.1 MPa. The apparatus used for the reactivity tests was described elsewhere.[26] 0.100 g of catalyst was loaded

in the center of the quartz tubular reactor and quartz wool was placed on both sides of the catalyst bed to hold the catalyst. The reactant gas consisting of CO, CH_3ONO and N_2 with a volume ratio of 1/6/33 was delivered at 110 °C with a gas hourly space velocity (GHSV) of 8,000 mL $g_{cat.}^{-1}$ h^{-1}. The compositions of the reactant gas and outlet products were monitored by an online Agilent 7890B gas chromatography equipped with a thermal conductivity detector (TCD) and a flame ionization detector (FID). The calculations of the turnover frequency (TOF), CO conversion, CH_3ONO conversion, DMC, methyl formate (MF) and dimethoxymethane (DMM) selectivity based on CH_3ONO reactant were shown in Supporting Information (SI).

3. Results and discussion

3.1 Catalytic performance of Pd/NaY and Pd-Mo/NaY catalysts for dimethyl carbonate synthesis

The catalytic performance of Pd/NaY and Pd-Mo/NaY catalysts in the gas-solid phase indirect oxidation of methanol to DMC is shown in Fig. 1. During the 30 h reactivity test, the Pd-Mo/NaY catalyst exhibited a higher conversion of CO and CH_3ONO compared to the reference Pd/NaY catalyst. The Pd-Mo/NaY catalyst showed stable CO conversion within 30 h, while the Pd/NaY catalyst exhibited a remarkable decline of CO conversion from 94% to 70%, suggesting a gradual deactivation of Pd/NaY catalyst. The high stability of the Pd-Mo/NaY catalyst is attributed to the presence of Mo promoter. Furthermore, it was observed that the selectivity of DMC on the Pd/NaY and Pd-Mo/NaY catalysts exhibited a steady increase of approximately 10%. Conversely, the selectivity of DMM and MF on both catalysts was decreased, which was possibly attributed to the reconstruction of Pd active sites.[8,13] A similar change of DMC selectivity was observed on other Pd/NaY and Pd/EMT catalysts.[8,11,13] The DMC selectivity of the Pd-Mo/NaY catalyst is lower than that of the Pd/NaY, which is resulted from the exhaustion of CO reactant at a different average CO conversion (98% on Pd-Mo/NaY vs. 87% on Pd/NaY).

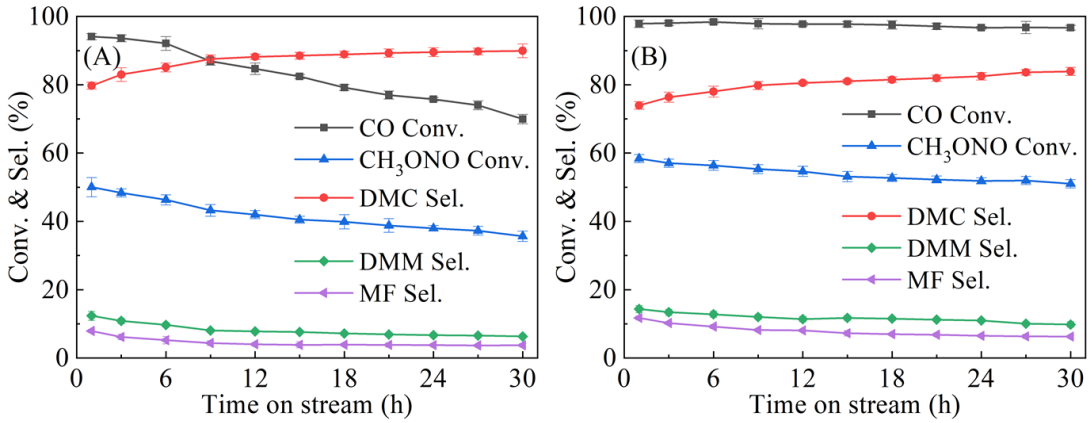

Fig. 1 Conversion of CO and CH_3ONO, selectivity of dimethyl carbonate (DMC), dimethoxymethane (DMM) and methyl formate (MF) over the catalysts (A) Pd/NaY and (B) Pd-Mo/NaY as a function of time on stream in the gas-solid phase indirect oxidation of methanol to DMC. Reaction conditions: 0.100 g catalyst, $CO/CH_3ONO/N_2$ = 1/6/33 (volume), GHSV = 8000 mL $g_{cat.}^{-1}$ h^{-1}, 110 °C, 0.1 MPa.

To reveal the reason for the low DMC selectivity change over the Pd-Mo/NaY catalyst (Fig. 1), the effect of the CO/CH_3ONO reactant ratio on the catalytic performance was investigated, and the results are shown in Fig. 2. When the CO/CH_3ONO ratio increased from 1/6 to 3/6, the CH_3ONO conversion progressively decreased due to the competitive adsorption of CO and CH_3ONO reactants following the Langmuir-Hinshelwood (L-H) mechanism of DMC formation,[12,27] while the DMC selectivity showed a volcanic-type variation tendency with a highest value of 86%. When the CO/CH_3ONO ratio was set at 1/6, the higher average CO conversion of 98% suggested the exhaustion of CO reactant, which resulted in a low DMC selectivity of about 80% on the Pd-Mo/NaY catalyst (Fig. 1B).

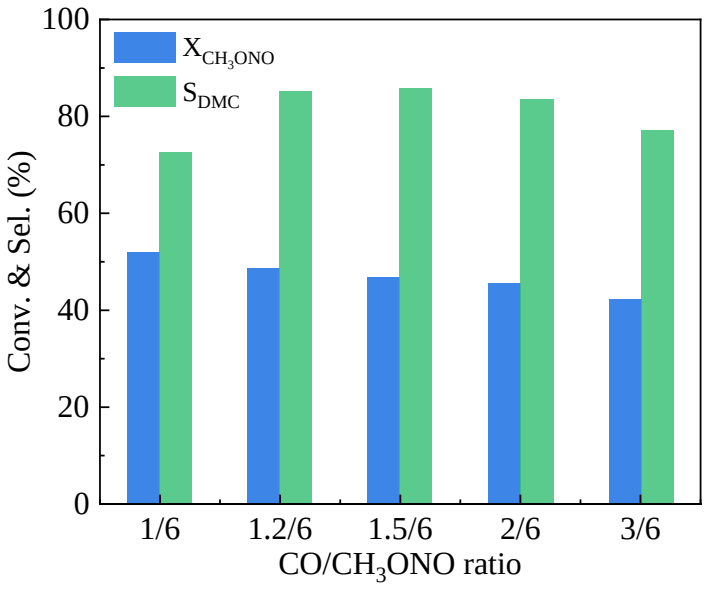

Fig. 2 Effect of the CO/CH_3ONO ratio on the CH_3ONO conversion and DMC selectivity over the Pd-Mo/NaY catalyst in the gas-solid phase indirect oxidation of methanol to DMC. Reaction conditions: 0.100 g catalyst, $CO/CH_3ONO/N_2$ = 1, 1.2, 1.5, 2, 3/6/33 (volume), GHSV = 8000–12000 mL $g_{cat.}^{-1}$ h^{-1}, 110 °C, 0.1 MPa.

The kinetics of catalysts was investigated after eliminating the influence of inner and outer diffusion (details provided in SI).[13,28] The apparent activation energies and turnover frequency (TOF) for the indirect oxidative carbonylation of methanol to DMC are shown in Table 1 and Fig. 3. The Pd-Mo/NaY catalyst exhibited a TOF of 0.019 s^{-1} at 110 °C, and Pd/NaY had a TOF of 0.005 s^{-1}. The difference of TOF is related to the introduction of the Mo promoter in the Pd-Mo/NaY catalyst. Pd/NaY and Pd-Mo/NaY catalysts show the activation energies of 72 kJ mol^{-1} and 87 kJ mol^{-1}, respectively. The comparable activation energies indicate that the reaction pathway and/or the rate-determining step are similar on the two catalysts.[8,29]

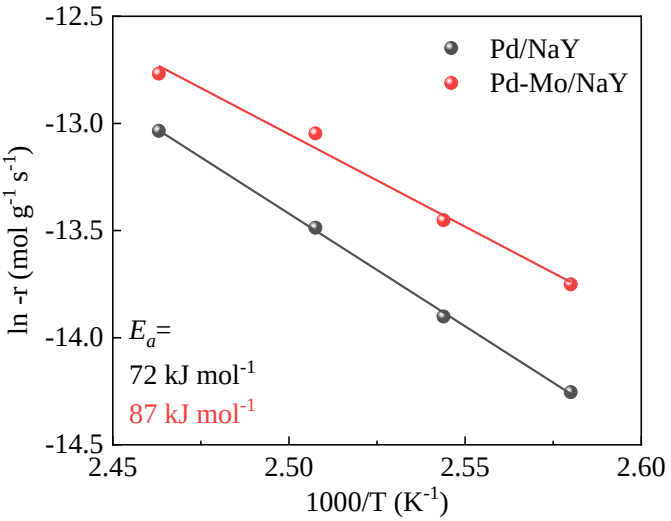

Fig. 3 Arrhenius plot for the DMC synthesis on the Pd/NaY and Pd-Mo/NaY catalysts (E_a, apparent activation energy). Reaction conditions: mixture of 0.010 g catalyst and 0.090 g α-Al_2O_3 (diluent), $CO/CH_3ONO/N_2$ = 1/6/33 (volume), GHSV = 80,000 mL $g_{cat.}^{-1}$ h^{-1}, 0.1 MPa.

Table 1 Physicochemical properties and catalytic performance of the Pd/NaY and Pd-Mo/NaY catalysts.

Catalyst	Status	S_{BET} (m^2 g^{-1})[a]	V_{mic} (cm^3 g^{-1})[a]	TOF (s^{-1})[b]	E_a (kJ mol^{-1})[c]
Pd/NaY	Fresh	887	0.33	0.005	72
Pd/NaY	After 30 h test	863	0.32	–	–
Pd-Mo/NaY	Fresh	857	0.32	0.019	87
Pd-Mo/NaY	After 30 h test	794	0.30	–	–

[a] Specific surface area measured by BET method and the micropore volume

determined by the *t*-plot method.

[b] Measured at 110 °C according to the CO conversion and Pd atoms (details provided in SI).

[c] Apparent activation energy calculated from the Arrhenius plot in Fig. 3 (details provided in SI).

3.2 Properties of fresh and used Pd/NaY and Pd-Mo/NaY catalysts

The XRD patterns of Pd/NaY and Pd-Mo/NaY catalysts before and after the catalytic test are presented in Fig. 4. The characteristic diffraction peaks of NaY zeolite are clearly observed at 6.2°, 15.6°, 20.3°, 23.4°, 27.0° and 31.3° 2Theta in all patterns.[13,16,19] The structure of the zeolite is well preserved after both the Mo incorporation and the catalytic test. In the enlarged XRD patterns presented in Fig. 4B, no diffraction peaks corresponding to palladium metal and palladium oxide are observed. This is due to the high dispersion and/or low content of Pd.[8,13]

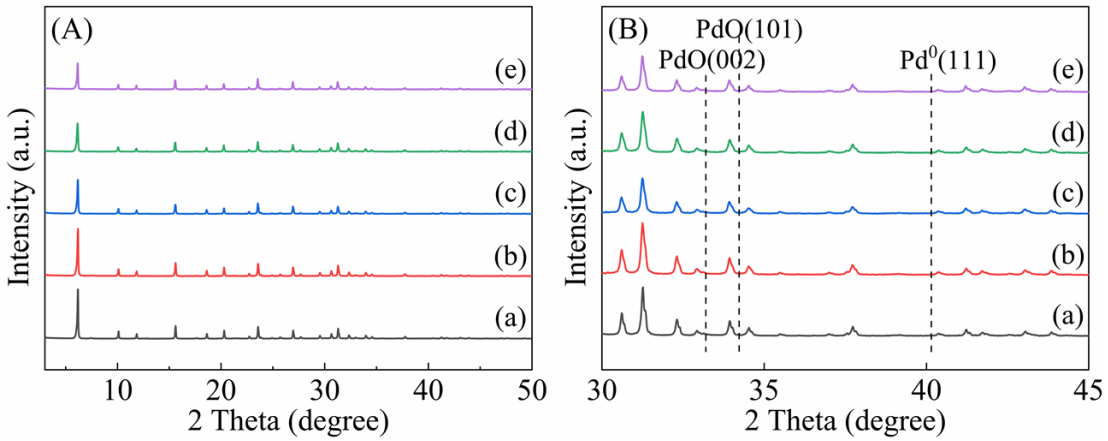

Fig 4. (A) XRD patterns in the range of 3-50° 2Theta and (B) enlarged patterns in the range of 30–45° 2Theta: (a) fresh Pd/NaY, (b) Pd/NaY after 30 h catalytic test, (c)

fresh Pd-Mo/NaY, (d) Pd-Mo/NaY after 30 h catalytic test, and (e) NaY zeolite.

The textural properties of the catalysts were examined by N_2 adsorption at –196 °C (Fig. S1 and Table 1). The adsorption profiles exhibit the Ⅰ-type isotherm typical for microporous materials.[30,31] The Pd/NaY and Pd-Mo/NaY samples before and after the catalytic test have similar specific surface areas of 794–887 m^2 g^{-1} and micropore volumes of 0.30–0.33 cm^3 g^{-1}. The similar micropore volumes suggest that the incorporation of Mo species has no effect on the zeolite structure. The N_2 adsorption-desorption results confirm that the textural properties of Pd/NaY and Pd-Mo/NaY catalysts do not affect their catalytic activity.

The weight loss of used Pd/NaY and Pd-Mo/NaY catalysts after 30 h catalytic test was measured by TG-MS analysis (Fig. S2). The amount of physically adsorbed water and residual reaction species in both catalysts were similar; no carbon was deposited on both catalysts. The results indicate that the deactivation of the Pd/NaY catalyst is not due to the residual reaction species or carbon deposits.

The morphology of both Pd/NaY and Pd-Mo/NaY catalysts is shown in Fig. S3. Both catalysts have an average crystal size of about 1.1 μm and similar morphology. The Pd nanoparticles are invisible in both Pd/NaY and Pd-Mo/NaY fresh catalysts by TEM (Fig. S4). After 30 h catalytic test, an abundant amount of Pd nanoparticles with an average size of 10.2 nm are observed on the external surface of the used Pd/NaY catalyst (Fig. 5). This is in a good agreement with the previous observation reported on Pd sintering that occurred during the synthesis of DMC.[8,13] Interestingly, the used

Pd-Mo/NaY catalyst showed a homogenous Pd distribution with an average size of 2.3 nm (Fig. 5). This observation is further confirmed by the SEM-EDS characterization of the Pd-Mo/NaY catalyst. The surface of the Pd/NaY catalyst contains randomly distributed Pd species (0.9–3.1 wt%) while the surface of the Pd-Mo/NaY catalyst is covered by homogenous Pd species (0.5–0.9 wt%) (Fig. 6). In accordance with the TEM, HAADF-STEM results indicate that sporadic Pd nanoparticles of about 6 nm are formed and most of them are highly dispersed (Fig. S5). HAADF-STEM-EDS elemental mapping revealed the high dispersion of Mo with a content of 0.3 wt%. The ICP-OES analysis confirmed the presence of Mo in the Pd-Mo/NaY catalyst of about 0.1 wt%. These results suggest that the addition of Mo hinders the aggregation of Pd species in sample Pd-Mo/NaY during the catalytic test, thus improving the stability of the catalyst.

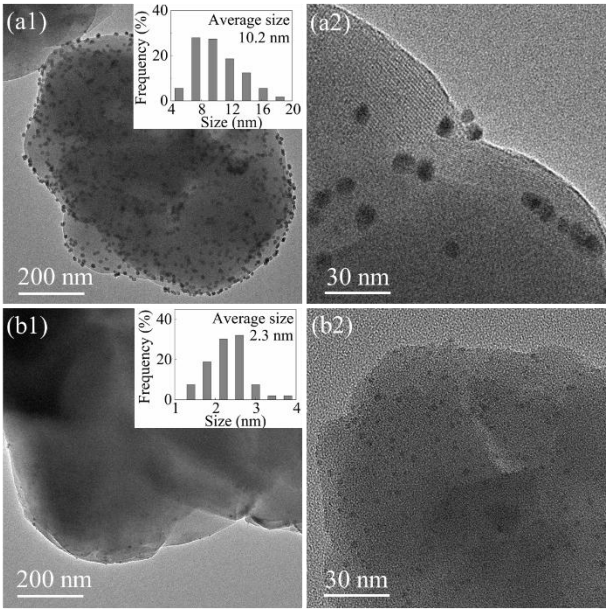

Fig. 5 TEM images of used catalysts after 30 h catalytic test: (a1, a2) Pd/NaY and (b1, b2) Pd-Mo/NaY. *Insets*: particle size distribution of Pd nanoparticles in samples Pd/NaY (a1) and Pd-Mo/NaY (b1) determined by measuring of about 200

nanoparticles.

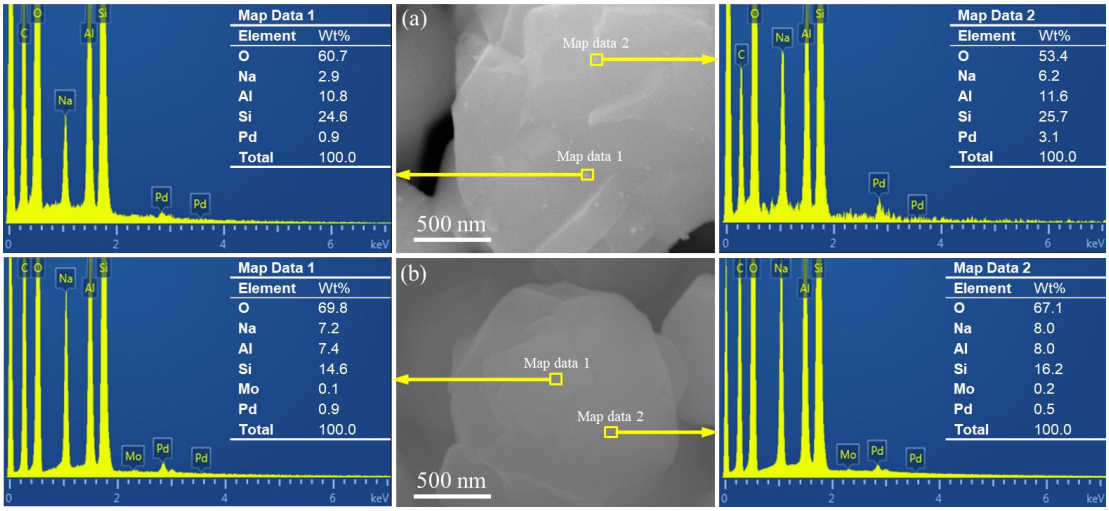

Fig. 6 SEM images and EDS elemental mapping of (a) Pd/NaY and (b) Pd-Mo/NaY used catalysts after 30 h catalytic test.

Additionally, the silanol groups in the catalysts were characterized by FT-IR spectroscopy; the OH stretching vibration region is depicted in Fig. 7. The band at 3734 cm^{-1} is originally assigned to the presence of isolated silanols.[21,32-34] The strong band at 3634 cm^{-1} in both spectra of samples Pd/NaY and Pd-Mo/NaY is corresponded to the acidic bridging hydroxyl groups.[35-37] The formation of Si(OH)Al is attributed to the Na^+ exchange by the NH_4^+ originated from the $Pd(NH_3)_4^{2+}$ precursor.[38-40] The intensity of the band at 3634 cm^{-1} in the spectrum of sample Pd-Mo/NaY is lower than that in sample Pd/NaY, suggesting that the amount of bridging hydroxyl groups decreased with the introduction of Mo in the Pd-Mo/NaY sample. The incorporation of Mo into the Pd-Mo/NaY inhibits the formation of the bridging OH sites. Besides, the surface acidity of both Pd/NaY and Pd-Mo/NaY

catalysts was investigated using pyridine probe molecule followed by FT-IR spectroscopy (Fig. S6) and NH_3-TPD (Fig. S7). The FT-IR results reveal that the amount of Brønsted acidic sites was decreased in the Pd-Mo/NaY catalyst (Fig. S6). The NH_3-TPD results suggest that the acidity in the Pd-Mo/NaY is weaker than of the Pd/NaY catalyst (Fig. S7). The FT-IR and NH_3-TPD results confirmed that the introduction of Mo modified the properties of the Pd-Mo/NaY catalyst, especially the acidity.

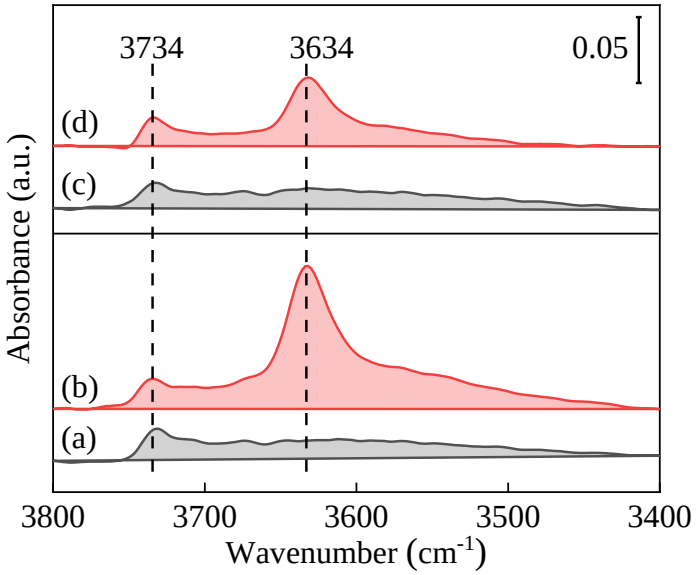

Fig. 7 FT-IR spectra of samples (a) NaY, (b) Pd/NaY, (c) Mo/NaY and (d) Pd-Mo/NaY in the OH stretching vibration region (3400–3800 cm^{-1}).

Further the properties of both catalysts in comparison to the zeolite support were studied by adsorption of CO followed by FT-IR spectroscopy. The CO with a partial pressure of 132–385 Pa was adsorbed at −140 °C on all samples NaY, Mo/NaY, Pd/NaY and Pd-Mo/NaY (Fig. 8). The bands at 2167 and 2169 cm^{-1} are assigned to the OH–CO, Na^+–CO or $Mo^{\delta+}$–CO ($4 \leq \delta \leq 6$) species, and the band at 2123 cm^{-1} is

attributed to physically adsorbed CO.[33,41-43] As the CO partial pressure increased from 132 Pa to 385 Pa, the intensities of the bands gradually enhanced. The intensities of the band at 2167 cm^{-1} at the different CO concentrations in the spectra of Mo/NaY are higher than in the NaY (Fig. 8C); similarly, the Pd-Mo/NaY was higher than Pd/NaY (Fig. 8F). This difference is due to the presence of Mo in both Mo/NaY and Pd-Mo/NaY samples.

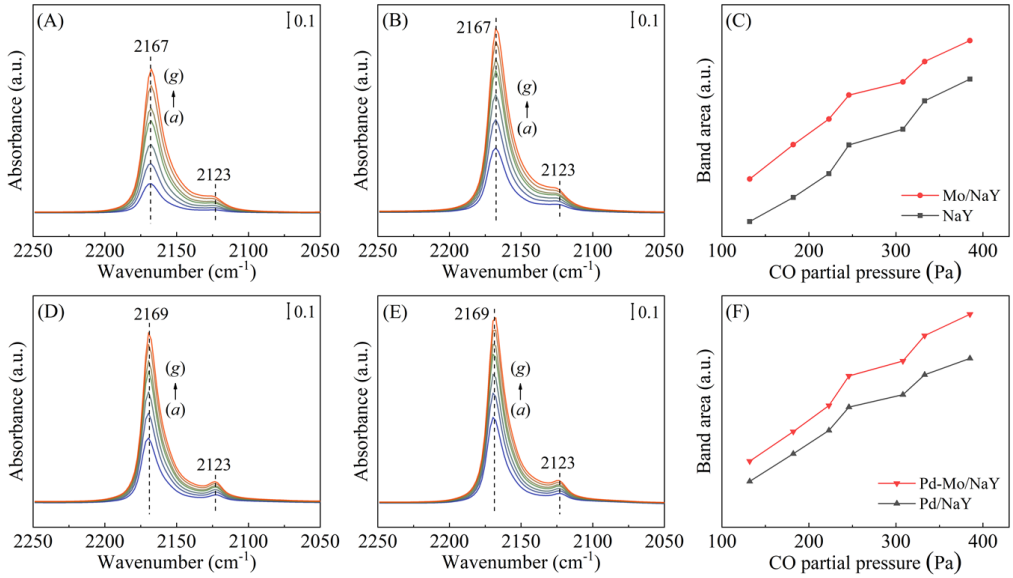

Fig. 8 FT-IR spectra of CO adsorbed at −140 °C on samples (A) NaY, (B) Mo/NaY, (D) Pd/NaY and (E) Pd-Mo/NaY. (C) The band areas at 2167 cm^{-1} versus the CO partial pressure. (F) The band areas at 2169 cm^{-1} versus the CO partial pressure. The spectra were collected at the equilibrium CO partial pressure of (a) 132 Pa – (g) 385 Pa.

On the basis of the above results, the high performance of Pd-Mo/NaY catalyst is initially explained by the introduction of Mo.

3.3 Inhibition of Pd sintering through Pd-Mo interactions

The adsorption of CO on the catalysts further was studied by DRIFTS. The DRIFTS spectra of CO adsorbed on both Pd/NaY and Pd-Mo/NaY used catalysts after 2 h and 6 h catalytic tests are shown in Fig. 9. The bands at 2119, 2094 and 2069 cm^{-1} are assigned to the CO adsorbed on the Pd^{2+} and Pd^{0} species, respectively.[39,44-46] And the band at 1988 cm^{-1} is attributed to the bridged CO adsorbed on Pd^{0} species.[8,47] The intensities of CO adsorption bands on the used Pd-Mo/NaY catalyst are much higher than that on the Pd/NaY after the catalytic test (2 h and 6 h). The enhanced CO adsorption on the Pd-Mo/NaY catalyst is associated with the high dispersion of Pd species, while the weak CO adsorption on the Pd/NaY catalyst is attributed to the aggregation of Pd species. This observation is consistent with the TEM results (Fig. 5). Thus the Mo promoter is found to inhibit the Pd sintering. The high dispersion of Pd species and the enhanced adsorption of CO are considered as key descriptors of the high stability of the catalysts.[47]

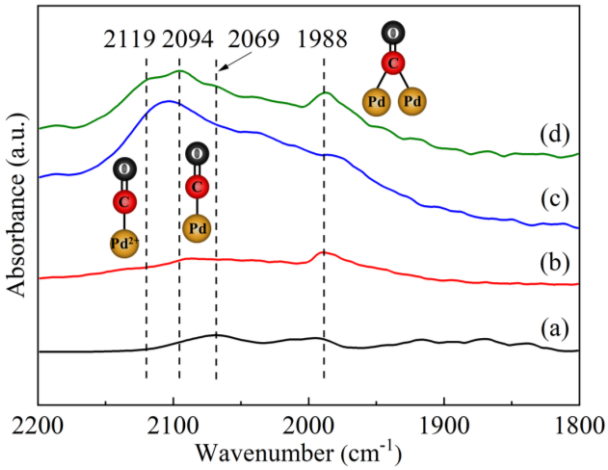

Fig. 9 DRIFTS spectra of CO adsorbed on used Pd/NaY catalysts after (a) 2 h and (b) 6 h catalytic test, and on used Pd-Mo/NaY catalysts after (c) 2 h and (d) 6 h catalytic

test recorded at 35 °C.

To investigate the redox properties of Pd/NaY and Pd-Mo/NaY catalysts, H_2-TPR experiments were conducted. As shown in Fig. 10, in comparison with Pd/NaY catalyst, the Pd-Mo/NaY catalyst exhibited two additional peaks at 448 and 506 °C associated with the reduction of Mo^{6+} to Mo^{5+} and Mo^{5+} to Mo^{4+}.[48-50] The high reduction temperature at 448 and 506 °C confirmed the presence of Mo. In addition, the peaks below 400 °C are assigned to the reduction of Pd^{2+} to Pd^0.[40,49] After Mo modification, the main reduction peaks are shifted from 133 °C to 170 °C and from 371 °C to 348 °C in the sample Pd-Mo/NaY. This shift of the reduction peaks of Pd species can be attributed to the Mo promoter through Pd-Mo interactions.

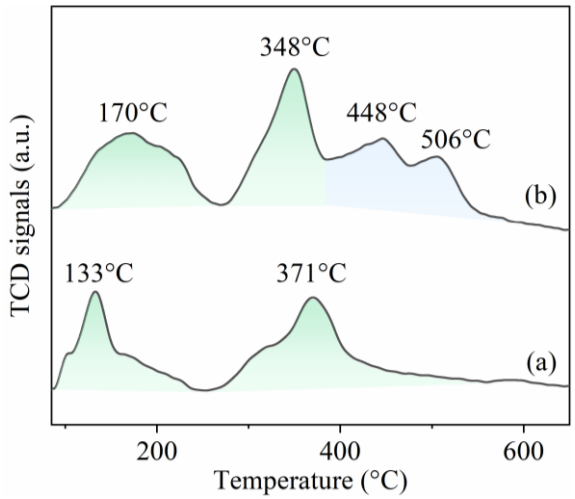

Fig. 10 H_2-TPR profiles of fresh (a) Pd/NaY and (b) Pd-Mo/NaY catalysts.

The state of Pd and Mo species was further studied by XPS (Fig.11). The binding energies at about 337.4 and 342.6 eV are ascribed to the Pd^{2+} species, and the binding energies at 335.8 and 341.0 eV are attributed to the Pd^0 (Fig.11A).[47,51,52] The

proportions of Pd^{2+} and Pd^{0} species are listed in Table 2. The peak area ratio of the Pd^{2+}/Pd^{0} is 1.6 for the Pd-Mo/NaY and 1.2 for the Pd/NaY catalysts. In the Pd-Mo/NaY catalyst, abundant Pd^{2+} species result from the presence of Mo promoter through the Pd-Mo interactions. The binding energies at 235.1 and 231.8 eV are assigned to Mo^{6+} species, and the binding energies at 233.5 and 230.3 eV are attributed to Mo^{5+} species in the Pd-Mo/NaY catalyst (Fig. 11B). No peaks corresponding to Mo species are detected in the spectrum of Pd/NaY catalyst.

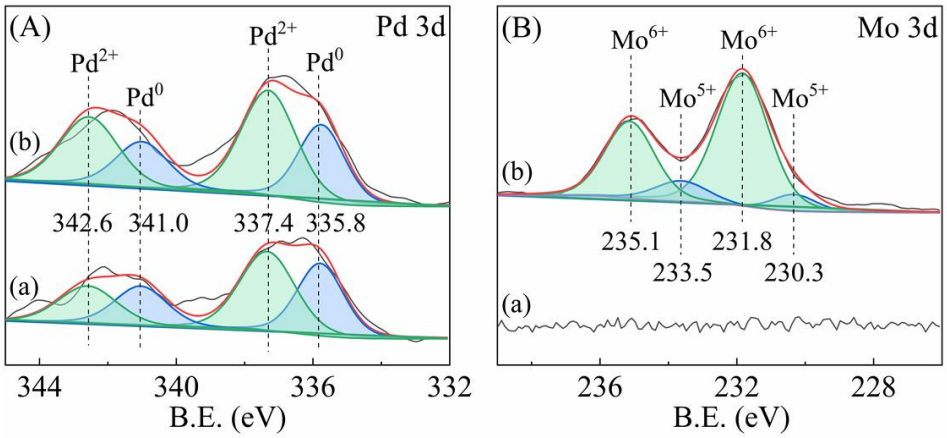

Fig. 11 XPS spectra of (A) Pd 3d and (B) Mo 3d regions of used catalysts (a) Pd/NaY and (b) Pd-Mo/NaY.

Table 2 The peak areas of Pd^{0}, Pd^{2+}, and Pd^{2+}/Pd^{0} area ratio of the used catalysts Pd/NaY and Pd-Mo/NaY determined by XPS.[a]

Catalyst	Area of Pd^{0}	Area of Pd^{2+}	Pd^{2+}/Pd^{0} ratio
Pd/NaY	1367[a]	1640[a]	1.2
Pd-Mo/NaY	1524[a]	2437[a]	1.6

[a] Peak areas of Pd^{0} at 335.8 eV and Pd^{2+} at 337.4 eV based on XPS spectra.

Furthermore, *in situ* DRIFTS experiments were conducted to investigate the

DMC synthesis over Pd/NaY and Pd-Mo/NaY catalysts. In Fig. 12A and 12B, the bands at 2963 and 2842 cm^{-1} are attributed to the anti-symmetric and symmetric C-H stretching vibrations;[12,19] The band at 2151 cm^{-1} corresponds to the linearly adsorbed CO species on the CH_3ONO-oxidized Pd^{2+} active sites;[12] The bands at 1780 cm^{-1} and 1322 cm^{-1} are assigned to the stretching vibrations of the C=O and C–O bonds belonging to DMC product;[14,53,54] The band at 1748 cm^{-1} is associated with the C=O stretching vibration of the reaction intermediate of $COOCH_3$*.[16,19] The multiple bands in the range of 1688–1612 cm^{-1} are assigned to the N=O vibrations of CH_3ONO reactant.[12,55] The band at 1461 cm^{-1} was assigned to C–H deformation vibrations of the CH_3–.[14,16,53] The bands at 1780 cm^{-1}, 1748 cm^{-1}, 1461 cm^{-1} and 1322 cm^{-1} appear in the spectrum recorded at 70 °C (Fig. 12A and 12B), suggesting the formation of DMC. As the temperature increases from 70 to 125 °C, the intensity of these bands gradually enhances due to the increased reaction rate.

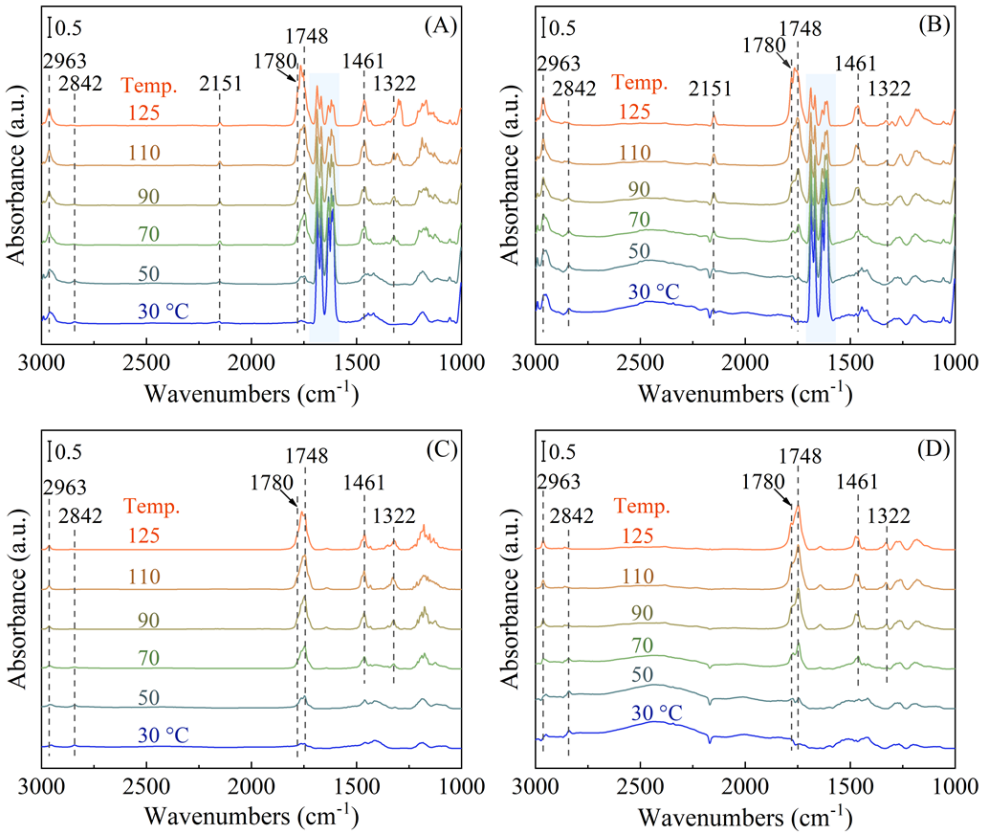

Fig. 12 *In situ* DRIFTS spectra of CO and CH_3ONO reactants on (A) Pd/NaY and (B) Pd-Mo/NaY catalysts, and the corresponding surface species on the (C) Pd/NaY and (D) Pd-Mo/NaY catalysts after parching with N_2 recorded at different temperatures: 30, 50, 70, 90, 110 and 125 °C.

Additionally, the Pd/NaY and Pd-Mo/NaY catalysts were purged with N_2 for 15 minutes to analyze the adsorbed surface species after being exposed to CO and CH_3ONO reactants (Fig. 12C and D). As the temperature increases from 70 to 125 °C, the intensity of the bands at 1780 cm^{-1}, 1748 cm^{-1}, 1461 cm^{-1} and 1322 cm^{-1} increases significantly, due to the increased reaction rate (Fig. 12A and B). The DRIFTS result confirms the existence of $COOCH_3$* reaction intermediate and demonstrated the similar reaction pathway and/or the rate-determining step on the

Pd/NaY and Pd-Mo/NaY catalysts. Moreover, it is worth noticing that the intensity of these bands at 2963 cm^{-1}, 2842 cm^{-1}, 2151 cm^{-1}, 1780 cm^{-1} and 1748 cm^{-1} on Pd-Mo/NaY is higher than that on Pd/NaY catalyst (Fig. 12 and Fig. S8). This suggests better catalytic activity of the Pd-Mo/NaY catalyst, which is consistent with the results of catalytic evaluation (Fig. 1).

The above results, i.e., the H_2-TPR, DRIFTS of CO adsorption and XPS results suggested that the Mo promoter tuned the Pd active sites on the Pd-Mo/NaY catalyst. The Pd-Mo interactions inhibited the sintering of Pd species and maintained the Pd^{2+} active sites. This should be responsible for the high stability of Pd-Mo/NaY catalyst in the indirect oxidation of methanol to DMC reaction.

4. Conclusions

In this study, we have developed a high-performance catalyst by modifying Pd/NaY with Mo, resulting in stable catalytic activity. The CO conversion on the Pd-Mo/NaY catalyst remained consistently high at 97% throughout a 30-hour test, while on the reference Pd/NaY catalyst, the CO conversion decreased from 94% to 70%. The turnover frequency on the Pd-Mo/NaY catalyst was 0.019 s^{-1}, significantly surpassing the Pd/NaY catalyst's rate of 0.005 s^{-1}. The *in situ* DRIFTS experiments verified the existence of $COOCH_3$* reaction intermediate and revealed the similar reaction pathway and/or the rate-determining step on the Pd/NaY and Pd-Mo/NaY catalysts. Our findings further demonstrate that the incorporation of Mo partially

healed silanols and inhibited the sintering of Pd species. The interactions between Pd and Mo species, along with the increased Pd^{2+} active sites, contributed to an enhanced adsorption of CO reactant on the Pd-Mo/NaY catalyst. The stabilization of active Pd^{2+} species was responsible for the high performance of the Mo-promoted Pd-Mo/NaY catalyst.

Acknowledgements

This project was financially supported by the National Key R&D Program of China (2022YFE0116000, 2022YFA1503400), National Natural Science Foundation of China (42072147, 21908246, 21975285 and 22175200), Key Research and Development Program (Major Scientific and Technological Innovation Project) of Shandong Province (2021ZLGX06) and Sino-French International Research Network (IRN) “Zeolites”.

References

1 S. Huang, B. Yan, S. Wang and X. Ma, Recent Advances in Dialkyl Carbonates Synthesis and Applications, *Chem. Soc. Rev.*, 2015, **44**, 3079-3116.

2 H. Tan, Z. Wang, Z. Xu, J. Sun, Y. Xu, Q. Chen, Y. Chen and G. Guo, Review on the Synthesis of Dimethyl Carbonate, *Catal. Today*, 2018, **316**, 2-12.

3 A. Abdalla and D. Liu, Dimethyl Carbonate as a Promising Oxygenated Fuel for Combustion: A Review, *Energies*, 2018, **11**, 1552.

4 Z. Wang, J. Sun, Z. Xu and G. Guo, CO Direct Esterification to Dimethyl Oxalate and Dimethyl Carbonate: The Key Functional Motifs for Catalytic Selectivity, *Nanoscale*, 2020, **12**, 2131-2214.

5 K. Kohli, B.-K. Sharma and C.-B. Panchal, Dimethyl Carbonate: Review of Synthesis Routes and Catalysts Used, *Energies*, 2022, **15**, 5133.

6 D. Kaiser, L. Beckmann, J. Walter and M. Bertau, Conversion of Green Methanol to Methyl Formate, *Catalysts*, 2021, **11**, 869.

7 A.-O. Esan, A.-D. Adeyemi and S. Ganesan, A Review on the Recent Application of Dimethyl Carbonate in Sustainable Biodiesel Production, *J. Clean Prod.*, 2020, **257**, 120561.

8 C. Wang, W. Xu, Z. Qin, H. Guo, X. Liu and S. Mintova, Highly Active Pd Containing EMT Zeolite Catalyst for Indirect Oxidative Carbonylation of Methanol to Dimethyl Carbonate, *J. Energy Chem.*, 2021, **52**, 191-201.

9 R. Guo, Z. Hou, J. Chen, Y. Qin, G. Chai and Y. Yao, Improved Catalytic Performance of Pd-Cu/NaY Zeolite by Tunning Al Distribution for the Synthesis

of Dimethyl Carbonate, *Fuel*, 2022, **330**, 125484.

10 A.-H. Tamboli, A.-A. Chaugule and H. Kim, Catalytic Developments in the Direct Dimethyl Carbonate Synthesis from Carbon Dioxide and Methanol, *Chem. Eng. J.*, 2017, **323**, 530-544.

11 Y. Yamamoto, T. Matsuzaki, S. Tanaka, K. Nishihira, K. Ohdan, A. Nakamura and Y. Okamoto, Catalysis and Characterization of Pd/NaY for Dimethyl Carbonate Synthesis from Methyl Nitrite and CO, *J. Chem. Soc., Faraday Trans.*, 1997, **93**, 3721-3727.

12 C. Wang, B. Liu, P. Liu, K. Huang, N. Xu, H. Guo, P. Bai, L. Ling, X. Liu and S. Mintova, Elucidation of the Reaction Mechanism of Indirect Oxidative Carbonylation of Methanol to Dimethyl Carbonate on Pd/NaY Catalyst: Direct Identification of Reaction Intermediates, *J. Catal.*, 2022, **412**, 30-41.

13 C. Wang, N. Xu, T. Liu, W. Xu, H. Guo, Y. Li, P. Bai, X. Wu, X. Gong, X. Liu and S. Mintova, Mechanical Pressure-Mediated Pd Active Sites Formation in NaY Zeolite Catalysts for Indirect Oxidative Carbonylation of Methanol to Dimethyl Carbonate, *J. Catal.*, 2021, **396**, 269-280.

14 H. Tan, Z. Wang, Z. Xu, J. Sun, Z. Chen, Q. Chen, Y. Chen and G. Guo, Active Pd(II) Complexes: Enhancing Catalytic Activity by Ligand Effect for Carbonylation of Methyl Nitrite to Dimethyl Carbonate, *Catal. Sci. Technol.*, 2017, **7**, 3785-3790.

15 S. Ji, Y. Chen, G. Zhao, Y. Wang, W. Sun, Z. Zhang, Y. Lu and D. Wang, Atomic-Level Insights into the Steric Hindrance Effect of Single-Atom Pd

Catalyst to Boost the Synthesis of Dimethyl Carbonate, *Appl. Catal., B*, 2022, **304**, 120922.

16 H. Tan, Z. Chen, Z. Xu, J. Sun, Z. Wang, R. Si, W. Zhuang and G. Guo, Synthesis of High-Performance and High-Stability Pd(II)/NaY Catalyst for CO Direct Selective Conversion to Dimethyl Carbonate by Rational Design, *ACS Catal.*, 2019, **9**, 3595-3603.

17 Y. Dong, Y. Shen, Y. Zhao, S. Wang and X. Ma, Synergy between Palladium and Potassium Species for Efficient Activation of Carbon Monoxide in the Synthesis of Dimethyl Carbonate, *ChemCatChem*, 2015, **7**, 2460-2466.

18 R. Guo, Y. Qin, L. Qiao, J. Chen, X. Wu and Y. Yao, Enhancement of the Catalytic Performance in Pd-Cu/NaY Catalyst for Carbonylation of Methyl Nitrite to Dimethyl Carbonate: Effects of Copper Doping, *Catal. Commun.*, 2017, **88**, 94-98.

19 S. Wu, R. Guo, J. Chen, R. Ye, Y. Qin, H. Wu, S. Zong, Y. Liu and Y. Yao, Rational Design of Ga-Substituted NaY Zeolites with Controllable Acidity for Remarkable Carbonylation of Methyl Nitrite to Dimethyl Carbonate, *Fuel*, 2023, **342**, 127756.

20 S.-V. Konnov, F. Dubray, E.-B. Clatworthy, C. Kouvatas, J.-P. Gilson, J.-P. Dath, D. Minoux, C. Aquino, V. Valtchev, S. Moldovan, S. Koneti, N. Nesterenko and S. Mintova, Novel Strategy for the Synthesis of Ultra-Stable Single-Site Mo-ZSM-5 Zeolite Nanocrystals, *Angew. Chem., Int. Ed.*, 2020, **59**, 19553-19560.

21 I.-C. Medeiros-Costa, E. Dib, N. Nesterenko, J.-P. Dath, J.-P. Gilson and S. Mintova, Silanol Defect Engineering and Healing in Zeolites: Opportunities to Fine-Tune Their Properties and Performances, *Chem. Soc. Rev.*, 2021, **50**, 11156-11179.

22 I.-C. Medeiros-Costa, E. Dib, F. Dubray, S. Moldovan, J. Gilson, J. Dath, N. Nesterenko, H.-A. Aleksandrov, G.-N. Vayssilov and S. Mintova, Unraveling the Effect of Silanol Defects on the Insertion of Single-Site Mo in the MFI Zeolite Framework, *Inorg. Chem.*, 2022, **61**, 1418-1425.

23 F. Dubray, S. Moldovan, C. Kouvatas, J. Grand, C. Aquino, N. Barrier, J. Gilson, N. Nesterenko, D. Minoux and S. Mintova, Direct Evidence for Single Molybdenum Atoms Incorporated in the Framework of MFI Zeolite Nanocrystals, *J. Am. Chem. Soc.*, 2019, **141**, 8689-8693.

24 Z. Liu, C. Shi, D. Wu, S. He and B. Ren, A Simple Method of Preparation of High Silica Zeolite Y and Its Performance in the Catalytic Cracking of Cumene, *J. Nanotechnol.*, 2016, **2016**, 1-6.

25 C.-A. Emeis, Determination of Integrated Molar Extinction Coefficients for Infrared Absorption Bands of Pyridine Adsorbed on Solid Acid Catalysts, *J. Catal.*, 1993, **141**, 347-354.

26 K. Huang, N. Xu, B. Liu, P. Zhang, G. Yang, H. Guo, B. Peng, C. Wang and S. Mintova, Crystalline Microporous MoVBiO Polyoxometalates for Indirect Oxidation of Methanol to Methyl Formate: Effects of Organic Additives on Crystals Size and Catalytic Performance, *ChemCatChem*, 2022, **14**, e202200528.

27 S. Hu, C. Xie, Y.-P. Xu, X. Chen, M.-L. Gao, H. Wang, W. Yang, Z.-N. Xu, G.-C. Guo and H.-L. Jiang, Selectivity Control in the Direct CO Esterification over Pd@UiO-66: The Pd Location Matters, *Angew. Chem., Int. Ed.*, 2023, e202311625.

28 I. Song, S.-W. Jeon, H. Lee and D.-H. Kim, Tailoring the Mechanochemical Interaction between Vanadium Oxides and Zeolite for Sulfur-Resistant $DeNO_x$ Catalysts, *Appl. Catal., B*, 2022, **316**, 121672.

29 Y. Wang, Z. Hu, W. Tian, L. Gao, Z. Wang and Z. Yuan, Framework-Confined Sn in Si-Beta Stabilizing Ultra-Small Pt Nanoclusters as Direct Propane Dehydrogenation Catalysts with High Selectivity and Stability, *Catal. Sci. Technol.*, 2019, **9**, 6972-6993.

30 H. Awala, J. Gilson, R. Retoux, P. Boullay, J. Goupil, V. Valtchev and S. Mintova, Template-Free Nanosized Faujasite-Type Zeolites, *Nat. Mater.*, 2015, **14**, 447-451.

31 W. Zhuang, X. Liu, L. Chen, P. Liu, H. Wen, Y. Zhou and J. Wang, One-Pot Hydrothermal Synthesis of Ultrafine Pd Clusters within Beta Zeolite for Selective Oxidation of Alcohols, *Green Chem.*, 2020, **22**, 4199-4429.

32 G.-N. Vayssilov, H.-A. Aleksandrov, E. Dib, I.-M. Costa, N. Nesterenko and S. Mintova, Superacidity and Spectral Signatures of Hydroxyl Groups in Zeolites, *Microporous Mesoporous Mater.*, 2022, **343**, 112144.

33 K. Chakarova, S. Andonova, L. Dimitrov and K. Hadjiivanov, FTIR Study of CO and N_2 Adsorption on [Ge]FAU Zeolites in Their Na- and H-Forms, *Microporous*

Mesoporous Mater., 2016, **220**, 188-197.

34 L. Lakiss, C. Kouvatas, J.-P. Gilson, H.-A. Aleksandrov, G.-N. Vayssilov, N. Nesterenko, S. Mintova and V. Valtchev, Unlocking the Potential of Hidden Sites in Faujasite: New Insights in a Proton Transfer Mechanism, *Angew. Chem., Int. Ed.*, 2021, **60**, 26702-26709.

35 E. Dib, E.-B. Clatworthy, L. Lakiss, V. Ruaux and S. Mintova, Hydroxyl Environments in Zeolites Probed by Deuterium Solid-State MAS NMR Combined with IR Spectroscopy, *Inorg. Chem. Front.*, 2022, **9**, 2964-2968.

36 Y. Hui, J. Zheng, Y. Qin, X. Du, Y. Zu, J. Yang, S. Sun, X. Gao, Z. Sun and L. Song, Insight into the Nature and the Transformation of the Hydroxyl Species in the CeY Zeolite, *Inorg. Chem. Front.*, 2022, **9**, 1354-1365.

37 K. Chakarova, E. Ivanova, K. Hadjiivanov, D. Klissurski and H. Knözinger, Co-Ordination Chemistry of Palladium Cations in Pd-H-ZSM-5 as Revealed by FTIR Spectra of Adsorbed and Co-Adsorbed Probe Molecules (CO and NO), *Phys. Chem. Chem. Phys.*, 2004, **6**, 3702-3709.

38 U. Obenaus, M. Dyballa, S. Lang, M. Scheibe and M. Hunger, Generation and Properties of Brønsted Acid Sites in Bifunctional Rh-, Ir-, Pd-, and Pt-Containing Zeolites Y Investigated by Solid-State NMR Spectroscopy, *J. Phys. Chem. C*, 2015, **119**, 15254-15262.

39 S.-A. Yashnik, G.-A. Urzhuntsev, A.-I. Stadnichenko, D.-A. Svintsitskiy, A.-V. Ishchenko, A.-I. Boronin and Z.-R. Ismagilov, Effect of Pd-Precursor and Support Acid Properties on the Pd Electronic State and the Hydrodesulfurization

Activity of Pd-Zeolite Catalysts, *Catal. Today*, 2019, **323**, 257-270.

40 S.-T. Homeyer and W.-M.-H. Sachtler, Elementary Steps in the Formation of Highly Dispersed Palladium in NaY: I. Pd Ion Coordination and Migration, *J. Catal.*, 1989, **117**, 91-101.

41 K. Chakarova, K. Hadjiivanov, G. Atanasova and K. Tenchev, Effect of Preparation Technique on the Properties of Platinum in NaY Zeolite: A Study by FTIR Spectroscopy of Adsorbed CO, *J. Mol. Catal. A: Chem.*, 2007, **264**, 270-279.

42 K. Hadjiivanov, H. Knözinger and M. Mihaylov, FTIR Study of CO Adsorption on Ni-ZSM-5, *J. Phys. Chem. B*, 2002, **106**, 2618-2624.

43 W. Wu, Z. Wu, C. Liang, X. Chen, P. Ying and C. Li, In Situ FT-IR Spectroscopic Studies of CO Adsorption on Fresh Mo_2C/Al_2O_3 Catalyst, *J. Phys. Chem. B*, 2003, **107**, 7088-7094.

44 J. Lee, J. Chen, K. Giewont, T. Mon, C. Liu, E.-A. Walker and E.-A. Kyriakidou, Effect of Cobalt Incorporation on the Stability of Ionic Pd in the Presence of Carbon Monoxide over Pd/BEA Passive NO_x Adsorbers, *Chem. Eng. J.*, 2022, **440**, 135834.

45 Q. Sun, B.-W.-J. Chen, N. Wang, Q. He, A. Chang, C.-M. Yang, H. Asakura, T. Tanaka, M.-J. Hülsey, C.-H. Wang, J. Yu and N. Yan, Zeolite-Encaged Pd-Mn Nanocatalysts for CO_2 Hydrogenation and Formic Acid Dehydrogenation, *Angew. Chem., Int. Ed.*, 2020, **59**, 20183-20191.

46 V. Muravev, A. Parastaev, Y. van den Bosch, B. Ligt, N. Claes, S. Bals, N.

Kosinov and E.-J.-M. Hensen, Size of Cerium Dioxide Support Nanocrystals Dictates Reactivity of Highly Dispersed Palladium Catalysts, *Science*, 2023, **380**, 1174-1179.

47 C. Wang, N. Xu, K. Huang, B. Liu, P. Zhang, G. Yang, H. Guo, P. Bai and S. Mintova, Emerging Co-Synthesis of Dimethyl Oxalate and Dimethyl Carbonate Using Pd/Silicalite-1 Catalyst with Synergistic Interactions of Pd and Silanols, *Chem. Eng. J.*, 2023, **466**, 143136.

48 I. Pedroarena, L. Grande, J.-J. Torrez-Herera, S.-A. Korili and A. Gil, Analysis by Temperature-Programmed Reduction of the Catalytic System Ni-Mo-Pd/Al_2O_3, *Fuel*, 2023, **334**, 126789.

49 Z. He, Z. He, D. Wang, Q. Bo, T. Fan and Y. Jiang, Mo-Modified Pd/Al_2O_3 Catalysts for Benzene Catalytic Combustion, *J. Environ. Sci.*, 2014, **26**, 1481-1487.

50 E. Mannei, F. Ayari, C. Petitto, E. Asedegbega Nieto, A.-R. Guerrero Ruiz, G. Delahay, M. Mhamdi and A. Ghorbel, Light Hydrocarbons Ammoxidation into Acetonitrile over Mo-ZSM-5 Catalysts: Effect of Molybdenum Precursor, *Microporous Mesoporous Mater.*, 2017, **241**, 246-257.

51 S. Peng, Z. Xu, Q. Chen, Z. Wang, D. Lv, J. Sun, Y. Chen and G. Guo, Enhanced Stability of Pd/ZnO Catalyst for CO Oxidative Coupling to Dimethyl Oxalate: Effect of Mg^{2+} Doping, *ACS Catal.*, 2015, **5**, 4410-4417.

52 W. Xing, J. An, J. Lv, F. Irshad, Y. Zhao, S. Wang and X. Ma, Highly Active Pd-Fe/α-Al_2O_3 Catalyst with the Bayberry Tannin as Chelating Promoter for CO

Oxidative Coupling to Diethyl Oxalate, *Chin. Chem. Lett.*, 2021, **32**, 796-800.

53 D. Lv, Z. Xu, S. Peng, Z. Wang, Q. Chen, Y. Chen and G. Guo, (Pd–$CuCl_2$)/γ-Al_2O_3: A High-performance Catalyst for Carbonylation of Methyl Nitrite to Dimethyl Carbonate, *Catal. Sci. Technol.*, 2015, **5**, 3333-3339.

54 H. Wu, Y. Qin, Y. Xiao, J. Chen, R. Guo, S. Wu, L. Zhang, J. Zhang and Y. Yao, Synergistic Lewis Acid and Pd Active Sites of Metal-Organic Frameworks for Highly Efficient Carbonylation of Methyl Nitrite to Dimethyl Carbonate, *Inorg. Chem. Front.*, 2022, **9**, 2379-2388.

55 S. Peng, Z. Xu, Q. Chen, Y. Chen, J. Sun, Z. Wang, M. Wang and G. Guo, An Ultra-low Pd Loading Nanocatalyst with High Activity and Stability for CO Oxidative Coupling to Dimethyl Oxalate, *Chem. Commun.*, 2013, **49**, 5718-5720.